ACUSTICA · acta acustica
Vol. 84 (1998) 929 ~~938~~ 946

Mechanics of the Contact Area Between a Violin Bow and a String. Part III: Parameter Dependence

R. Pitteroff and J. Woodhouse*
Cambridge University Engineering Department, Trumpington St, Cambridge CB2 1PZ, U.K.

Summary
This paper explores aspects of the simulation model of a string bowed by a bow of finite width developed in the companions [1, 2] to this paper. In particular we study the details of the stick-slip transitions, the flattening effect, and the influence of changing bow-hair compliance and string bending stiffness. Modelling of the finite width changes markedly the region of the player's control-parameter space in which musically acceptable waveforms are obtained. It is clearly important to allow for finite-width effects in future systematic studies of bowed-string dynamics. It is shown that one can go some way towards doing this by defining an "equivalent point-bow model" in which use is made of the finite-width results to modify the friction model used in point-bow simulations.

PACS no. 43.75.De, 43.40.Cw

1. Introduction

In Parts I and II [1, 2] of this series of papers a model has been developed for the process of exciting a string by bowing, allowing for the finite size of the contact region between bow and string. In Part II we illustrated some general features of the results of finite-width simulations. Much of the discussion was directed towards the events occuring during the nominal sticking phase, particularly the "partial slips" in which some bow-hairs slip while others continue to stick. In this paper we will examine some of the other details of finite-width simulations, discuss some parameter studies and investigate effects arising from the deflection of the string in the plane perpendicular to the bowing plane.

We deal first with two effects which are familiar from studies using point-bow models: the maximum bow force and the flattening effect. If the bow force exceeds a certain threshold, Helmholtz motion is no longer possible. Below this level, high bow forces can produce a delay in the time of release which is still compatible with Helmholtz motion. If this delay is not compensated by an equally large advance in the time of capture, the result is flattening: the pitch of the played note is lower than the nominal pitch of the string. Flattening tends to be strongest at large bow force and when playing in high positions on low strings. Flattening is readily audible and usually undesirable.

The flattening effect has received significant scientific attention in recent years. It is an effect which is easily observed, which emerges from numerical experiments and which to an extent lends itself to analytical treatment. Bouasse [3] reported the earliest known measurements. Further measurements have been published by Faure and Boutillon [4] and Schumacher [5]. McIntyre and Woodhouse [6] explained the effect, at least within the framework of point-bow models, in terms of hysteresis in the frictional behaviour between bow and string. They used time-domain arguments, and supported their account with simulation results (which were in fact the earliest simulations of transient bowed-string motion). More recently Boutillon [7] used a different analytical approach to show some of the parameter dependence of the flattening phenomenon.

The flattening effect and the maximum acceptable bow force are both intrinsically linked to the physics of the stick-to-slip and slip-to-stick transitions of the Helmholtz motion, so it is convenient to discuss them together. The first issue concerns frictional behaviour. All results of numerical and analytical calculations are particular to the form of the friction law employed in the calculations. The exact form of this friction law is still unknown, if indeed the real frictional behaviour can be usefully described by a single friction law. It is difficult to measure the friction law directly, but attempts have been made to observe it indirectly. The approach is to adjust the form of the theoretical friction law to obtain a best fit of theoretical predictions to experimental data from real bowing [5]. When this approach is tried using the present finite-width model, it will be found that the result is significantly different than that using a point-bow model.

Next, in Section 4, we examine the influence on simulated solutions of changes in bow-hair impedance. The calculations performed in Part I showed clearly that finite bow-hair impedance has a strong influence on the reflection and transmission of waves incident on a bow at rest. We now investigate simulated bowed-string motion in which we vary the bow-hair impedance. Such a parameter study is important for various reasons: in reality the impedance changes over the length of the bow, and in any case the assumptions on which our estimate of the impedance is based may not always be applicable. Guettler [8] reports that allowing for bow-hair compliance in point-bow models can lead to shorter starting transients. Here the concern is with the effect on finite-width simulations of steady-state Helmholtz motion.

In Section 5 we deal with the influence on simulated solutions of bending stiffness of the string in the vicinity of the bow. The evanescent fields arising from bending stiffness

Received 17 June 1996,
accepted 17 September 1997.

* To whom correspondence should be sent

ACUSTICA · acta acustica
Vol. 84 (1998)

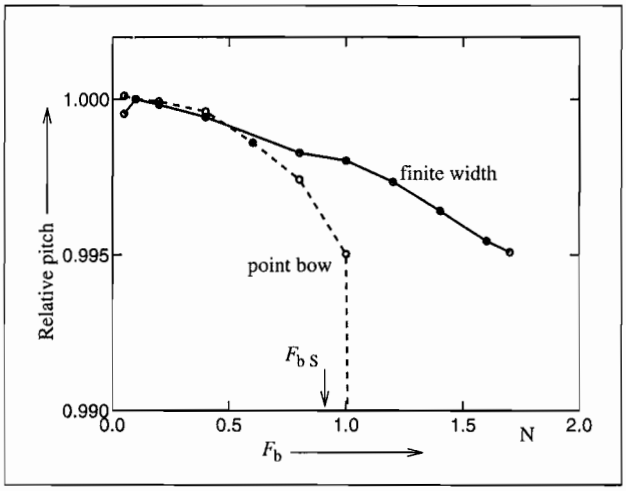

Figure 1. Flattening predicted by the point-bow and the finite-width models versus bow force F_b. Pitch relative to pitch at $F_b = 0.1$ N. The maximum bow force according to Schelleng's rule (Part II, equation (18)), is denoted F_{bS}.

are likely to have a length-scale comparable to that of the actual Helmholtz corner and to the bow width. We will see that bending stiffness affects the details of the release and capture mechanisms more than it affects the partial slips.

Players constantly alter the angle at which the ribbon of bow hair is tilted in the plane perpendicular to the bowing plane, presumably to change the bow-force distribution and the effective width of the bow. In Section 6 we assess first the possible range of non-uniformity in the bow-force distribution resulting from the static interaction of bow and string. We then investigate the effects of non-uniform bow-force distribution on the motion of the bowed string. Finite-width-related effects pertaining to the motion of the string in the perpendicular plane are also considered.

All simulations in this paper employ the string and bowing parameters given in Section 3.1 of Part II unless explicitly stated otherwise. The bow is modelled by the simple "spring-dashpot" model with distributed spring constant s and damping constant d.

2. Flattening and maximum bow force

Some computed results are shown in Figure 1. The relative pitch is plotted as a function of bow force F_b for a point-bow and a finite-width model. Pitch is understood simply as the inverse of the period length determined by counting the number of time steps between successive stick-to-slip transitions. The results are taken from simulations with constant bow force, initialised with the waveforms of idealised Helmholtz motion and run until a sufficiently steady-state regime has been attained. The results shown are averages over periods 50–100. Averaging is necessary because of small period-to-period fluctuations in period length: fluctuations of numerical origin are inevitable when the underlying period length is not an integer multiple of the time step, and fluctuations of physical origin may occur due to the extreme sensitivity of these systems to small disturbances. The pitch is given relative to the pitch at $F_b = 0.1$ N. This compensates the small, bow-force independent difference between the nominal period length T_0 and the computed period length. This difference, a feature of the discretisation schemes employed in the numerical models, was discussed in Part II, Section 3.3. The relative bowing position β of the point-bow is that of the mid-point of the finite-width bow. In the point-bow case the distributed bow-hair impedance of the finite-width bow is concentrated in a single point.

The finite-width model predicts a substantially smaller degree of flattening than the point-bow model (Figure 1). The maximum bow force, the threshold beyond which Helmholtz motion fails, is markedly higher for the finite-width model. There are various routes into non-acceptable motion as the bow force increases. To be acceptable, the motion must be near-periodic, but a general criterion separating acceptable from non-acceptable motion is hard to formulate [9]. For the point-bow model and the parameters of the reference case, the occurrence of main slips with durations $T_{slip} < \beta T_0$, indicating the failure of Helmholtz motion, seems to provide an adequate definition of the maximum bow force. So defined, $F_{b\,max} \approx 0.8$ N for the point bow. Above this value of bow force a transition from periodic to aperiodic motion takes place. For $F_b > 1.1$ N the model predicts highly aperiodic, raucous motion.

The finite-width model continues to produce Helmholtz motion for levels of bow force beyond the point-bow maximum bow force (and indeed higher than those shown in the graph) but with an increasing intensity of irregularities caused by partial slips. The criterion $T_{slip} < \beta T_0$ yields $F_{b\,max} \approx 1.4$ N. This criterion may lead to overestimates of $F_{b\,max}$ for finite-width models: the appearance of spikes in the bridge-force waveform, which in the present example occurs for $F_b < 1.4$ N, might render a regime, formally Helmholtz motion, musically non-acceptable. In any case, there is probably not a clear line between acceptable and non-acceptable. The musical context may also matter: what is acceptable for a concerto soloist may not be desirable in a string quartet.

Why do the two models behave so differently? First, recall how the solution to the motion of the bowed string is obtained in the rigid point-bow algorithm of McIntyre and Woodhouse [6]. The friction force F and the string surface velocity v are related in two different ways, which together determine their values at a given time t. First, from the linear-system behaviour of the string, the applied force generates an additional component of surface velocity which is simply proportional to the force:

$$v - v_{in} = \frac{F}{2Z}, \tag{1}$$

where Z is the characteristic impedance of the string for forces applied to its surface, and v_{in} is the velocity generated at the bowing point by incoming waves arising from earlier excitation of the string. If v_{in} is known, this is the equation of a straight line in the (v, F)-plane, for example the dashed line with slope $2Z$ in Figure 2.

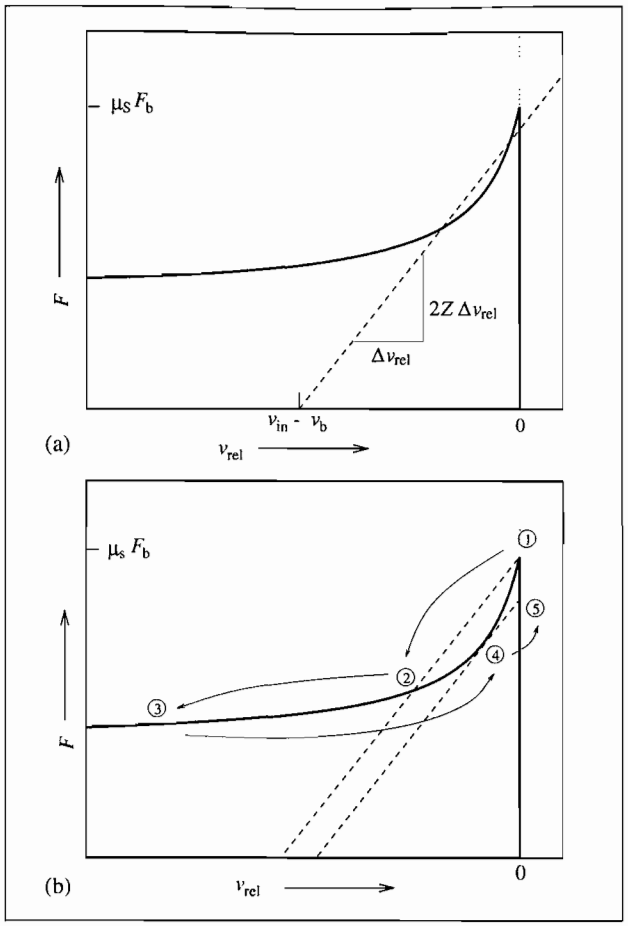

Figure 2. The graphical solution of the two equations determining friction force F and surface velocity v of the bowed point in a rigid point-bow model.

The second relation between F and v comes from the assumed friction law. For the simple model of rosin friction in use here, F is a nonlinear function of the relative velocity v_{rel} between bow-hair and string surface, of the kind indicated by the solid line in Figure 2. When $v_{\mathrm{rel}} = 0$, there is sticking friction and F may take any value between the limits determined by the coefficient of static friction μ_S and the bow force F_b. When $v_{\mathrm{rel}} \neq 0$, F is assumed to vary according to equation (2),

$$F = \mu(v_{\mathrm{rel}})\, F_b\,, \tag{2}$$

which relates F to the coefficient of dynamic friction μ and F_b. The values of F and v can be obtained by the graphical solution represented in Figure 2(a). For a rigid bow $v = v_{\mathrm{rel}} + v_b$, for a compliant bow $v = v_{\mathrm{rel}} + v_b + v_H$, where v_H is the velocity of the bow-hair at the point of contact, relative to the velocity v_b of the bow stick.

The intersection of the sloping line and the velocity axis, marked $v_{\mathrm{in}} - v_b$, is the instantaneous value of the string surface velocity at the bowing point resulting from the incoming waves, minus the bow velocity. If the maximum slope of the friction curve is greater than $2Z$ an ambiguity can arise from multiple intersections of the friction curve and the sloping line, as shown in the figure. For a given friction *law* $\mu = \mu(v_{\mathrm{rel}})$, the maximum slope of the friction *curve* depends linearly on the bow force F_b. McIntyre and Woodhouse [6] showed that the correct resolution of this ambiguity is a hysteresis loop in the (F,v_{rel})-plane. The solution point jumps quasi-instantaneously from the top of the vertical part of the friction curve, marked "1" in Figure 2(b) to the intersection marked "2". Subsequently the magnitude of the relative velocity increases to "3". Towards the end of the slipping phase the magnitude of the relative velocity decreases and the solution point climbs up the friction curve to point "4" from where it jumps back to the vertical part of the friction curve at "5". This hysteresis behaviour produces the flattening effect. In general, the larger the hysteresis loop the stronger the flattening. Larger hysteresis loops are the result of a higher bow force or a steeper friction law.

The finite-width model offers no graphical representation which we can interpret in a similar way. If one plots the local friction force of a single "hair" against the local relative velocity there is no hysteresis loop. The natural analogue to the (F, v_{rel})-plane of the point bow would be to use spatially averaged quantities: the total friction force and the relative velocity averaged across the width of the bow. A plot of these quantities which corresponds to Figure 2(b) is shown in Figure 3(a). The solid line connects successive solution points, i.e. pairs of friction force and relative velocity at given times. The circles indicate solution points at intervals of $T_0/278$. The dashed line is the friction law used in the computations. The spatially averaged quantities provide us with an idea of what friction law would be "seen" by finite-width velocity and force transducers.

The total friction force never reaches the nominal value of limiting friction $\mu_s F_b$ because the release of the string has a finite duration and different sections of the string under the bow attain limiting friction at different times. The averaged solution point performs a small hysteretic loop in the (F, v_{rel})-plane due to the asymmetry of the release and capture process. In addition, partial slips produce an apparent second branch of the friction law. The underlying friction law and the one "seen" by the imagined finite-width transducer differ strongly. The relative velocity is difficult to observe in an experiment, whereas the string centre-line velocity and the bow velocity can be measured straightforwardly. Figure 3(b) therefore shows the total friction force versus the averaged centre-line velocity v_c offset by the bow velocity v_b. The qualitative picture is the same.

The same effects are visible in waveforms of the friction force. Figure 4 compares the waveforms of local values of the friction force with the total friction force. The rather violent activity at discrete points under the bow is completely masked by the averaging. The strong qualitative differences between the local values of the friction force and the total value suggest that when approaching the topic of friction forces experimentally one would be best advised to work with force transducers with widths small compared to the bow width. Güth [10] attempted to measure the friction force by inserting a piezo-electric transducer sensitive to longitudinal forces between the full-width ribbon of bow-hair and the frog of the bow. In the light of these simulation results his rather

ACUSTICA · acta acustica
Vol. 84 (1998)

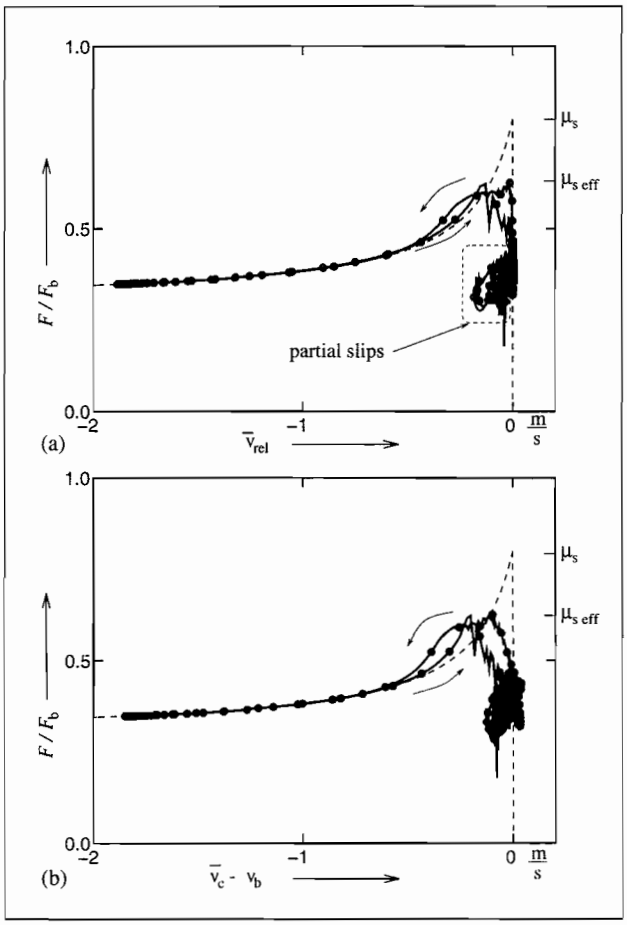

Figure 3. "Effective" friction laws. Total friction force F (normalised with bow force F_b) versus (a) averaged relative velocity and (b) averaged string centre-line velocity v_c offset by the bow velocity v_b. The dashed line represents the friction law actually used. (See text.)

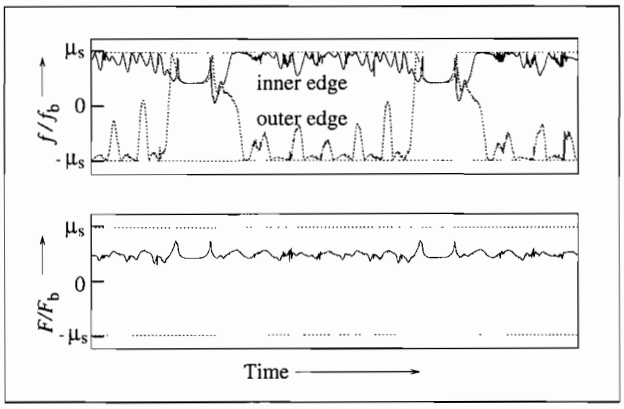

Figure 4. Local and averaged friction forces between bow and string. The top traces are the friction forces at the two edges of the bow, the lower trace shows the force integrated across the width of the bow. Time window $2\,T_0$.

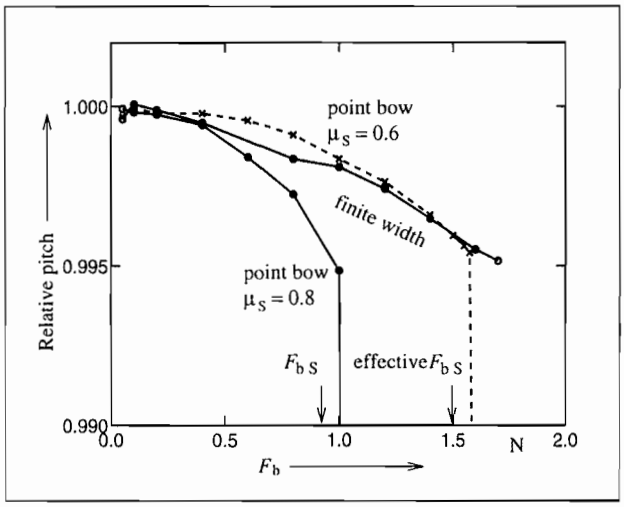

Figure 5. Flattening predicted by the point-bow model using the "effective" point-bow friction law and by the point-bow and the finite-width models as above. Note the "effective" $F_\mathrm{b\,S}$, the theoretical maximum bow force calculated with $\mu_\mathrm{s\,eff}$.

strong statements about the frictional behaviour of the bow and string contact seem open to question. If the bottom trace of Figure 4 were a measured time series of the friction force, then, in the spirit of conventional point-bow methodology, one would deduce a coefficient of static friction of $\mu_\mathrm{s} \approx 0.6$, clearly reduced from the $\mu_\mathrm{s} = 0.8$ used in the computation. This discrepancy makes clear that inferring a friction law from measurements performed on a real bowed string is not a straightforward task.

We may, however, infer an "effective" point-bow friction law from the finite-width results. The simplest approach is to replace the coefficient of static friction μ_s in the friction law by an "effective" coefficient $\mu_\mathrm{s\,eff}$. To test this approach, we run the point-bow model with $\mu_\mathrm{s} = 0.6$ whilst keeping all other input parameters unchanged. The results of this calculation are seen in Figure 5. We find flattening behaviour and a maximum bow force much more similar to what was found in the original finite-width calculation. (This observation may also resolve an apparent conflict with the work of Schumacher [5]. He reported good agreement between experiments and point-bow simulations, but his simulations were probably based on an "effective" friction law in the sense defined here.)

If point-bow arguments apply to the finite-width case in an approximate way then we can argue that because $(\mu_\mathrm{s\,eff} - \mu_\mathrm{d}) < (\mu_\mathrm{s} - \mu_\mathrm{d})$ there is a smaller hysteretic area in the (F, v_rel)-plane and therefore less flattening. Insertion of $\mu_\mathrm{s\,eff}$ into Schelleng's maximum bow-force rule (see Part II equation (18)) leads to an "effective" theoretical maximum bow force $F_\mathrm{b\,S}$ which matches the value produced by the finite-width model quite well (Figure 5). Main slips with durations $T_\mathrm{slip} < \beta\,T_0$ occur for $F_\mathrm{b} > 1.2$ N.

The value of $\mu_\mathrm{s\,eff}$ deduced from a plot like Figure 3 is bow-force dependent. For very small bow force, $\mu_\mathrm{s\,eff} \approx \mu_\mathrm{s}$. As F_b increases $\mu_\mathrm{s\,eff}$ drops quickly. For $F_\mathrm{b} > 0.3\,F_\mathrm{b\,max}$ there is little change.

If finite-width results differ so strongly from point-bow results, then one may also want to know how changes in bow width affect the behaviour of the finite-width model. There are two suitable numerical experiments: change of b while keeping constant the values of s and d, the distributed spring

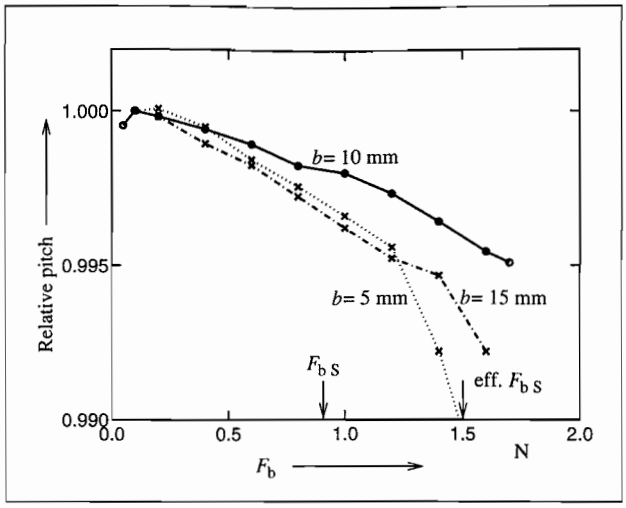

Figure 6. Flattening as a function of bow width.

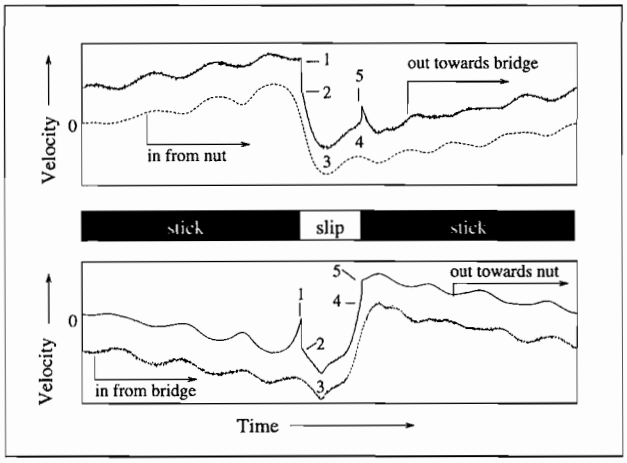

Figure 7. Shaping of velocity waves by the action of the point bow during release (top) and capture (bottom). Dashed and solid lines are incoming and outgoing surface-velocity waves respectively. Time window T_0.

and damping constants, which is probably what happens in real bowing; or change of b while keeping constant the values of $s\,b$ and $d\,b$ which emphasises the contribution of the change in geometry. The results of the first experiment are presented in Figure 6. As the bow width is reduced the finite-width model shows flattening behaviour more and more similar to the point-bow model. This is due to both the reduction in bow width and the reduction in total bow-hair impedance, an effect to be discussed in the next section. For $b = 5\,\mathrm{mm}$ one finds $\mu_{\mathrm{s\,eff}} \approx 0.75$ at $F_\mathrm{b} = 0.4\,\mathrm{N}$. Increased flattening is also observed for bow widths greater than the standard value of $b = 10\,\mathrm{mm}$ used throughout. For $b = 15\,\mathrm{mm}$ one finds $\mu_{\mathrm{s\,eff}} < 0.6$ at $F_\mathrm{b} = 0.4\,\mathrm{N}$. The explanation for increased flattening despite the flatter "effective" friction law is the following: flattening tends to increase when, all other parameters being equal, bowing further away from the bridge. In Part II Section 4.2 we developed the notion of an "effective" bowing point (or "effective" β). This is the bowing point for the point-bow model, all other parameters being equal, which produces the bridge-force waveform most similar to that of the finite-width model. The effective bowing point was found to lie between the mid-point of the bow and the outer edge, in that part of the bow where the string sticks to the bow permanently throughout the sticking phase. Therefore an increase in bow width about a fixed bow mid-point moves the effective bowing point further away from the bridge, and so contributes to flattening.

To a first approximation this behaviour can be summarised in the following way. If b is small then an increase in b produces a major reduction in $\mu_{\mathrm{s\,eff}}$ and a minor shift away from the bridge of the effective bowing point, so the result is reduced flattening. If b is large then an increase in b produces a minor reduction in $\mu_{\mathrm{s\,eff}}$ and a major shift away from the bridge of the effective bowing point, so the result is increased flattening. If minimal flattening is an optimisation criterion for bow design, then for the parameters of our reference case, which were chosen to be realistic, $b \approx 10\,\mathrm{mm}$ is optimal.

3. Release and capture

The fingerprints of hysteresis are readily seen in the shapes of waveforms of the string velocity. The physical processes of the stick-to-slip and slip-to-stick transitions become apparent in the changes a wave undergoes as it passes through the bow. The wave to monitor when investigating the stick-to-slip transition is the velocity wave approaching the bow from the nut and leaving the bow in the direction of the bridge. Velocity waves are understood here as the left- and right-going waves at a given point in space which, superimposed, give the velocity at this point. The string surface velocity, i.e. centre-line velocity offset by the rotational velocity, gives the clearest picture. Conversely, for the slip-to-stick transition the information-carrying wave is the velocity wave approaching the bow from the bridge and leaving the bow in direction of the nut. This applies to both point-bow and finite-width results, shown in Figures 7 and 8 respectively. In these graphs incoming waves are given by dashed lines and outgoing waves by solid lines. As an indicator of the timing of release and capture the corresponding friction maps are shown as well.

As the rounded corner of the velocity wave returning from the nut approaches the outer edge of the bow the incoming velocity wave begins its negative swing (Figure 7 top graph) but sticking persists. This leads to a delay of the transition. In terms of the graphical solution of Figure 2(b) this process corresponds to the intersection point moving up the vertical part of the friction curve. The numbers shown in Figure 7 correspond to those in Figure 2(b). The delay and the subsequent discontinuous jump of the intersection point in the (F, v_{rel})-plane from the top point of the friction curve to the intersection on the slip branch of the friction curve give the outgoing velocity wave its characteristic sharp shape. At capture a second, much smaller, jump takes place, as can be inferred from the graphical solution shown in Figure 2(b). Comparison of the incoming and outgoing waves in Figure 7, bottom graph, shows sharpening of the velocity wave as it

ACUSTICA · acta acustica
Vol. 84 (1998)

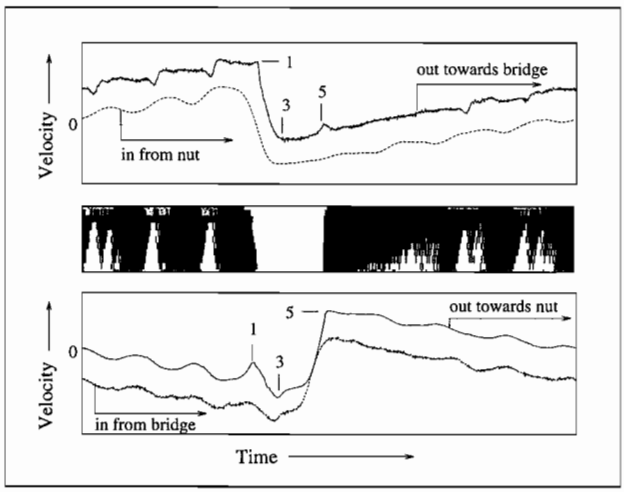

Figure 8. Shaping of velocity waves by the action of the finite-width bow during release (top) and capture (bottom). Dashed and solid lines are incoming and outgoing surface-velocity waves respectively. Time window T_0.

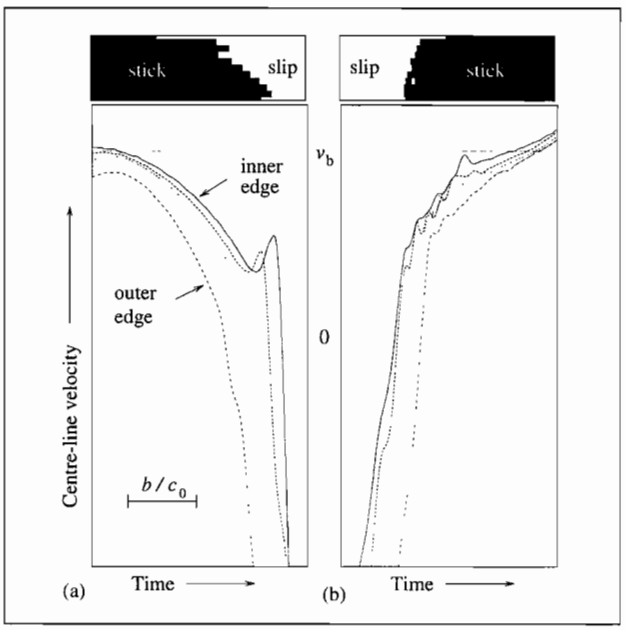

Figure 9. Close-up of (a) release and (b) capture for the finite-width model. Centre-line velocity at five equidistant grid-points under the bow versus time. Time windows of $0.05\,T_0$ each. Note the progressive steepening of the Helmholtz corner in (a) as it passes the bow.

passes the bow and an advance of the slip-to-stick transition. The delay at release offset by the advance at capture determines the lengthening of the period.

In the case of the finite-width model (Figure 8) the incoming and the outgoing waves are naturally time-separated due to the width of the bow. Sharpening of the rounded corner is clearly visible but to a lesser extent than in the point-bow case. As a result of the gradual unzipping as opposed to the instantaneous jumps of the point-bow model the discontinuity (1) is followed by a non-vertical section. The waveform at capture (5) is much rounder than in the point-bow case. The release delay is of smaller magnitude than in the point-bow case. (To appreciate the magnitude of this delay the travel time of a transverse perturbation crossing the bow width, $b/c_0 \approx 0.03\,T_0$, must be subtracted out.)

Let us now zoom in even further on release and capture. The five lines in Figure 9 are the centre-line velocities at five equidistant points under the bow. The curves are naturally time-separated and thus the order from the outer to the inner edge is clearly visible. The duration of the stick-to-slip transition is close to b/c_0. Near the outer edge the incoming Helmholtz corner suffers only minor changes in shape. As the Helmholtz corner progresses further into the bow, the friction force is built up at each "bow-hair", the waveform is sharpened and eventually local stick-to-slip transitions are triggered. The timing of each discrete release can be read off the friction map and is found to correspond to the point of maximum curvature in the waveform at each point.

The difference between string centre-line velocity and bow velocity v_b prior to the individual release is partly due to rolling of the string and partly due to differential bow-hair stretching. Capture also takes place gradually but usually far more rapidly than release. It is more difficult to locate the event of capture in velocity waveforms than the event of release.

4. Sensitivity to bow-hair parameters

The bow-hair parameters used throughout are based on the measurements of material properties described in Part I, and on the assumptions that only one layer of bow-hair is involved in bowing and that the dynamics of the bow-stick plays only a minor role. The relevant argument concerning the bow stick is that differential motion of hairs is largely independent of the dynamic behaviour of the bow stick. The good agreement found in Part I between the experimental data on the reflection and transmission problem and the predictions based on the above assumptions is encouraging. However, this does not preclude the possibility that there are bowing situations in which these assumptions are inadequate.

It may well be that at high bow force more than one layer of bow-hair is affected by the friction force. Equally it may be that at low bow force and when the bow is tilted, less than one full layer of bow-hair is affected by the friction force. As few as 10 and as many as 200 hairs could be involved in bowing. On the other hand, if the one-layer assumption holds but bow-stick dynamics were to turn out to be a determining feature in a certain situation, then the impedance used throughout this study would be too high.

Let z_{H0} be the distributed bow-hair impedance of the reference case with the values of the spring and damping constants s and d used throughout (see Part II Section 3.1). These values correspond to a sheet of 50 hairs with width $b = 10$ mm on a violin bow. In this section we study three model bows with $z_H/z_{H0} = 0.25,\ 1,\ 4$ so that the range of uncertainty concerning the number of effective hairs is covered. One may think of the model bows as representing "violin bows" with 13, 50 and 200 hairs. For point-bow models $Z_H = b\,z_H$.

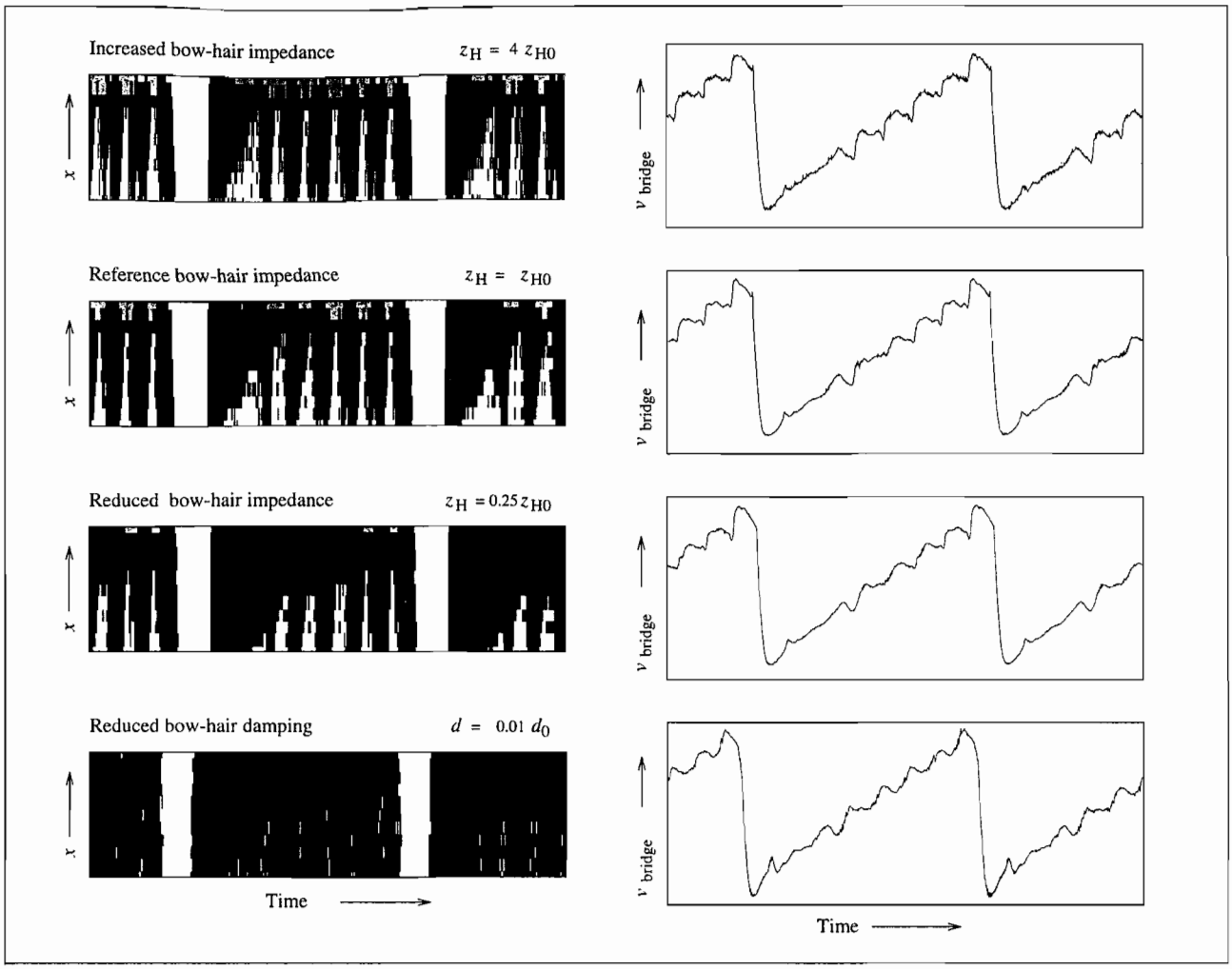

Figure 10. Effect of altered bow-hair impedance on friction map and bridge-force waveform. Time window $2\,T_0$.

Figure 10 shows friction maps and bridge-force waveforms for the three model bows. A more compliant bow can accommodate a higher degree of incompatibility between the velocities of bow and string because it allows differential bow-hair stretching to a higher degree. This is why, as the bow is made more compliant, the partial slips as seen in the friction maps diminish in intensity. The changes in the friction maps are reflected in smoother bridge-force waveforms. In this example, the partial slips can be made to vanish by lowering the impedance to $z_H = 0.05\, z_{H0}$. The bottom pictures in Figure 10 will be discussed shortly.

The compliance dependence of the flattening behaviour is shown in Figure 11. Let us begin with the point-bow model. Figure 11(a) presents the relative pitch for the three point bows versus bow force. Changes in bow-hair impedance produce little variation in maximum bow force and flattening. There is a very weak tendency towards increased flattening on more compliant bows. A second effect connected with the change in compliance is related to the transition from acceptable Helmholtz motion ($F_b < 0.8$ N) to highly aperiodic raucous motion ($F_b > 1.1$ N) as the bow force increases. In all three point-bow cases there is a clear bow-force threshold at $F_b = 1.0$ N beyond which there is an intermediate regime of strong flattening (3%, approximately a quarter-tone), before highly aperiodic raucous motion takes over. However, only in the most compliant case is this intermediate regime sufficiently periodic to qualify as non-raucous. This is perhaps because the greater losses associated with the more compliant bow enhance the stability of the periodic motion.

As before in the reflection and transmission problem (Part I), changes in compliance affect the results of finite-width models more than those of point-bow models (Figure 11(b)). The change in behaviour with change in compliance is not monotonic and this rules out simple explanations. The two finite-width cases with $z_H = 1\, z_{H0}$ and $z_H = 4\, z_{H0}$ continue to produce Helmholtz motion for levels of bow force higher than the point-bow models but with an increasing intensity of irregularities in the ripple patterns and increasing fluctuations in period length. These are strongest on the least compliant bow. The results suggest that the upper limit of acceptable bow-hair impedance lies below $z_H = 4\, z_{H0}$ for the violin bow. The most compliant case produces results qualitatively very similar to those of the point bows. Its maximum bow force is higher than that of the point bow, but it exhibits the same transition to the intermediate regime of strong flattening and then to raucous motion.

ACUSTICA · acta acustica
Vol. 84 (1998)

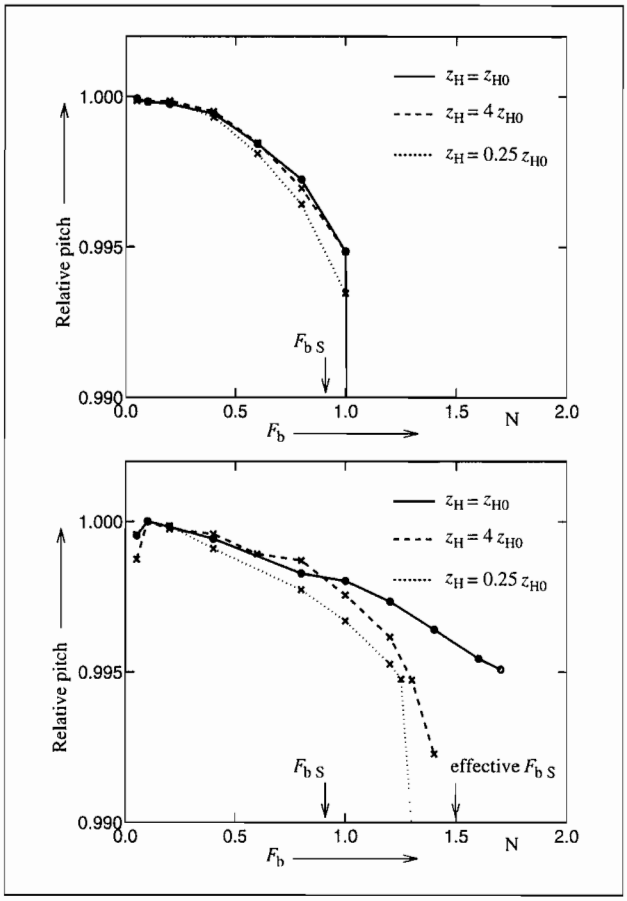

Figure 11. Compliance-dependent flattening: (a) point-bow and (b) finite-width model.

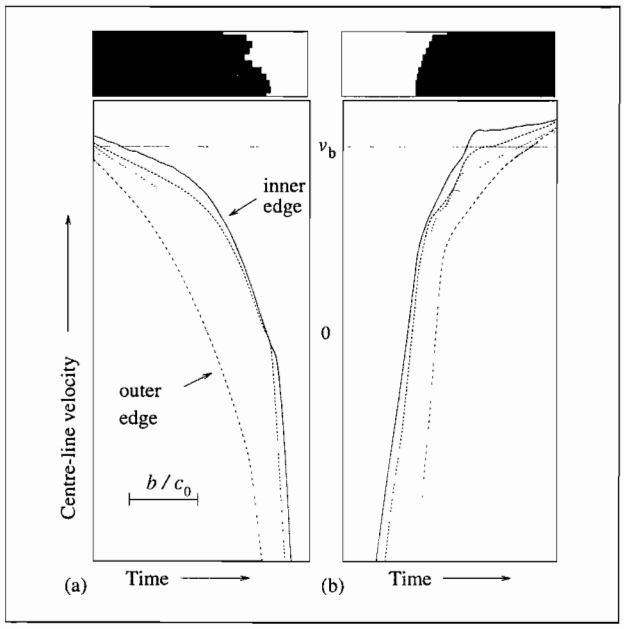

Figure 12. Close-up of (a) release and (b) capture for the finite-width model with the bow-hair impedance reduced to 0.25 of what is used throughout. Centre-line velocity at five equidistant grid-points under the bow versus time. Time windows of $0.05\,T_0$ each. Note that by comparison with Figure 9 there is less steepening of the velocity wave in (a) as it passes the bow.

On a real violin, discontinuous downward shifts in fundamental frequency by as much as an octave can be produced with high bow-force levels and this effect has recently entered contemporary composition for the violin [11]. Hanson *et al.* [12] have studied such an effect, christened "anomalous low frequency," in experimental work and Guettler [13] has presented numerical simulations using a *rigid* point-bow model. Such a regime with anomalous low frequency is produced by the finite-width case with $z_H = 0.25\,z_{H0}$ for $F_b > 2\,\mathrm{N}$. The present effect is clearly linked to bow-hair compliance, which is not the case with Guettler's results obtained with a rigid point-bow model.

The effect of reduced bow-hair impedance on the details of release and capture can be seen in Figure 12. The results compare with those of the reference case seen in Figure 9. Here the bow-hair impedance is reduced by a factor of 4. If the bow is very compliant then the arrival of the rounded corner of the Helmholtz waveform does not immediately trigger release. As a consequence the Helmholtz corner receives less sharpening. The strong delay at release is not counterbalanced by an advance at capture. This is consistent with the increase in flattening for the more compliant bow discussed above.

One may ask what happens if the spring and damping constants are changed independently. Within the range of uncertainty concerning the bow-hair impedance given above, changes of the damping constant are found to have a more important effect than changes of the spring constant. A change in the damping constant affects the real part of the bow-hair impedance only. The effect is largest at high frequency where the imaginary part of the impedance is small due to its $1/\omega$ dependence. On a violin many of the interesting physical effects are high-frequency effects. As a general rule lower values of the damping constant lead to fewer and less vigorous partial slips, smoother bridge-force waveforms and shorter main slips. Flattening behaviour is only changed very slightly.

The influence of the value of the damping constant on partial slips is interesting. Consider a high-frequency perturbation incident on the inner edge of the sticking bow, with a phase such that it leads to an increase in friction force. In cases with high damping constant this perturbation causes a sharp increase in friction force close to the edge of the bow. If prior to the arrival of the perturbation the level of the friction force at the edge was sufficiently high then the perturbation triggers a partial slip. Frequently the partial slip "propagates" further into the bow causing slipping over a large fraction of the bow width. This usually gives the bridge-force waveform sharp features. This is the type of behaviour known from the reference case.

With a lower damping constant the increase in friction force is not concentrated at the edge of the bow. This allows an incoming perturbation to progress into the bow without necessarily triggering slipping at the edge. Slipping is triggered wherever the local value of the friction force prior to the arrival of the perturbation was sufficiently close to limiting friction without, however, producing a propagating slip.

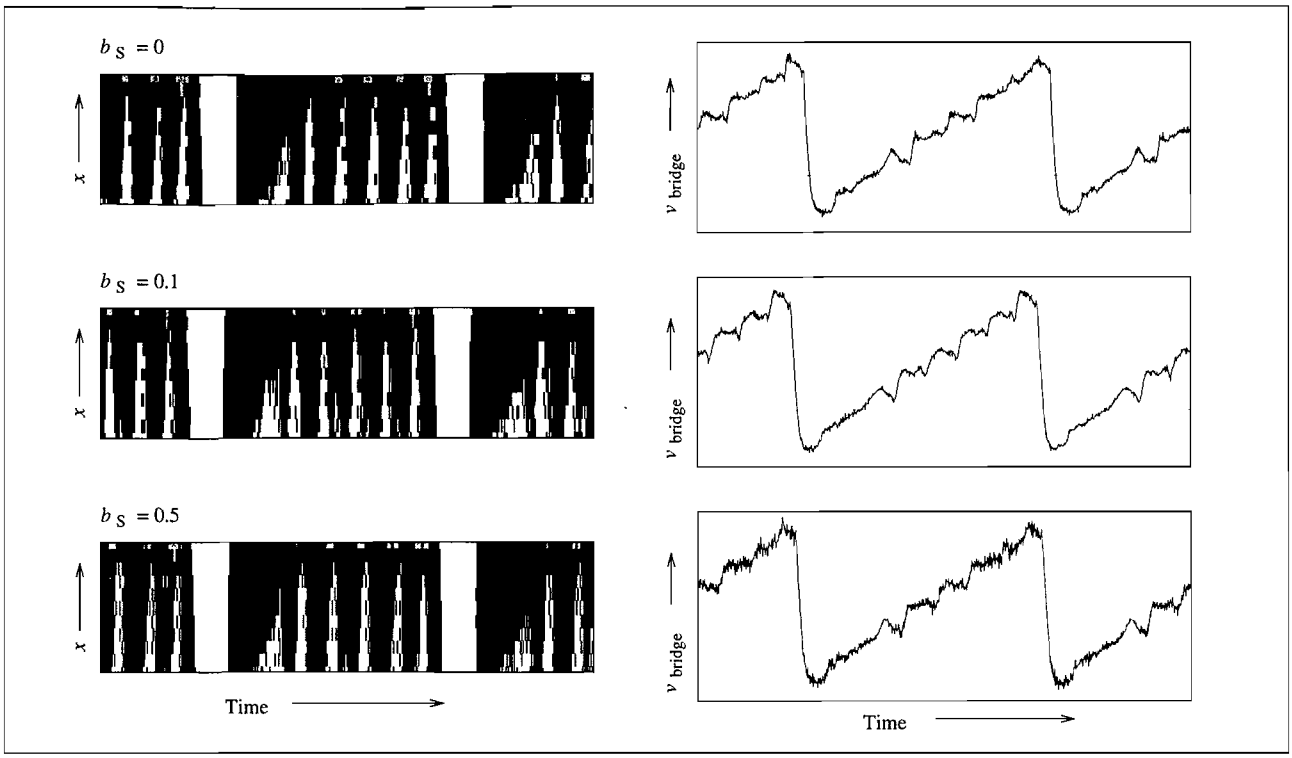

Figure 13. Friction maps and bridge-force waveforms for varying bending stiffness. Time window $2\,T_0$

Such behaviour is seen in the last example in Figure 10 where the damping constant is $d = 10$ (kg/s)/m, one hundredth of the value used throughout. Localised slips take place at individual "numerical hairs".

One conclusion drawn in Part I was that for the (linear) problem of the string sticking to the bow it seems more important to allow for compliance than finite width. This is especially necessary to model accurately the increased permeability of the bow at high frequency. In the context of the bowed string it seems to be crucial to allow for finite width, but less crucial to pick the precise bow-hair impedance. However, as in the linear problem, we find that finite-width models exhibit stronger compliance-related changes in behaviour than point-bow models.

5. Effect of bending stiffness

The treatment of bending stiffness requires rather important changes to the "perfectly flexible" simulation model used so far. We find that the predictions calculated with the "stiff" model with zero bending stiffness differ from those calculated with the "perfectly flexible" model in subtle ways. As we are investigating minute details these differences may be mistaken for physical effects. To avoid this, our reference case for the present section will be calculated using the "stiff" simulation model with zero bending stiffness. As stiffness parameter we choose Schelleng's [14] inharmonicity parameter b_S, with values $b_S = 0,\ 0.1,\ 0.5$. If the model string is thought of as solid and homogeneous then these values of b_S correspond to Young's moduli of 0, 5 and 35 GPa.

For a general picture, bridge-force waveforms and friction maps are given in Figure 13 for three cases with increasing bending stiffness. The numerical noise, most clearly visible in the bottom bridge-force plot, must not be interpreted as a physical phenomenon. The overall frictional pattern is not changed radically by the influence of bending stiffness. The duration of the main slip increases slightly with increase in stiffness.

The prominent effect of bending stiffness concerns the details of the main release, shown in Figure 14. The behaviour computed for the $b_S = 0$ case, Figure 14(a), closely resembles the behaviour calculated with the "perfectly flexible" model (Figure 9). High bending stiffness (Figure 14(b)) clearly leads to rounding of the waveform The shape of the Helmholtz corner arriving at the outer edge is not radically different from that of the $b_S = 0$ case. However, the Helmholtz corner receives very little sharpening as it passes the bow so the waveform emanating from the inner edge is very different from that of the $b_S = 0$ case. The unzipping process is shortened by approximately 50%: due to bending stiffness the restoring force builds up to the value of limiting friction more quickly. The details of capture differ in a much less fundamental way.

We now turn to the flattening behaviour, shown in Figure 15. For $b_S = 0$ the "stiff" model predicts flattening of the same order as the "perfectly flexible" model (see Figure 1). The general picture is that bending stiffness reduces the amount of flattening, although the effect is rather small when the bending stiffness is within Schelleng's recommended limit.

ACUSTICA · acta acustica
Vol. 84 (1998)

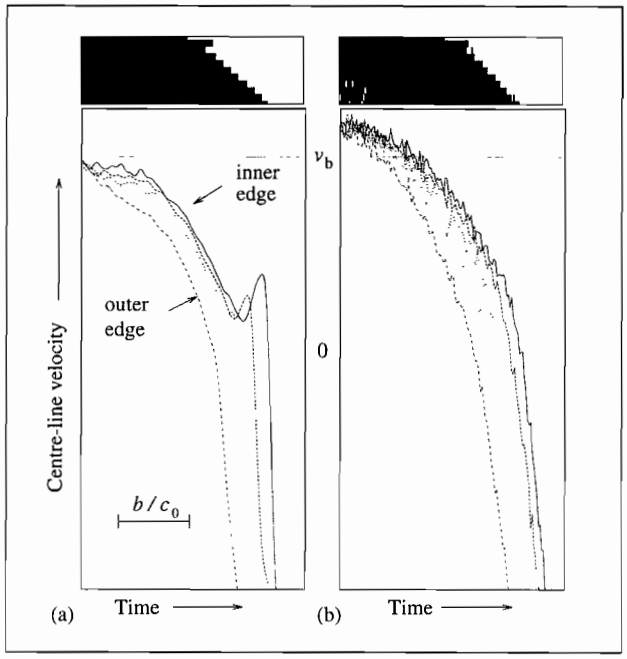

Figure 14. Details of release for (a) the $b_S = 0$ case and (b) the $b_S = 0.5$ case. String centre-line velocity versus time for five equidistant points under the bow. The stiff case shows weaker corner sharpening and an accelerated unzipping process. Time windows of 0.05 T_0 each.

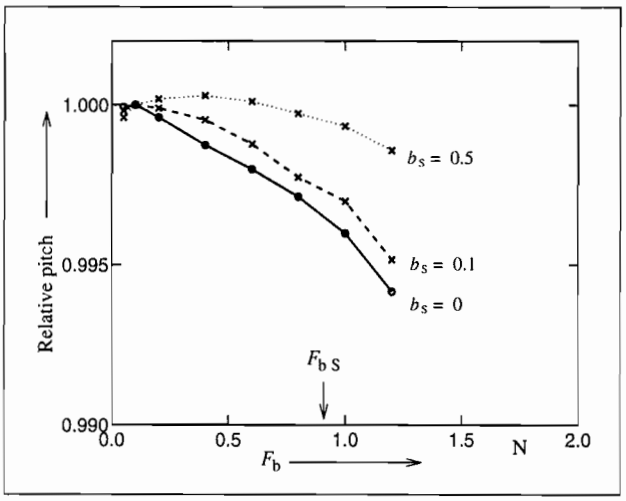

Figure 15. Relative pitch versus bow force predicted by the "stiff" finite-width model.

6. Effects pertaining to the perpendicular plane

The assumption of a uniform bow-force distribution used so far is certainly not tenable in all bowing situations. The static bow-force distribution must clearly depend on the angle at which the bow is tilted. It is also linked to the deformation of bow-hair and string in the plane *perpendicular* to the bowing plane. A schematic representation of the contact of bow and string is given in Figure 16.

In real bowing the bow force is perturbed by a variety of dynamic effects. The static bow force is modified by

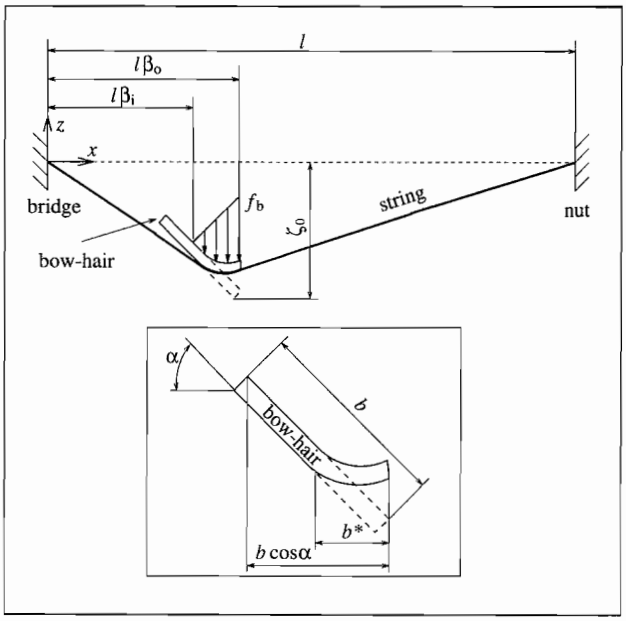

Figure 16. Schematic representation of the string and bow-hair deflection in the perpendicular plane. The dashed line represents the position of the bow-hair if the striing was removed.

the vibration of the bow in the perpendicular plane. Such bow vibration excites transverse waves on the string in the perpendicular plane. After reflection at the terminations of the string these waves return to the bow and contribute further to bow-force fluctuations. A second source of waves in the perpendicular plane is related to the kinematics of the bridge. When transverse waves impinge on the bridge, reflected waves are generated with components in both the bowing and the perpendicular plane [15, 16]. These two reflected waves reach the bow again and generate forces in the two planes. In particular, the Helmholtz corner, returning to the bow after reflection at the bridge, and its companion in the perpendicular plane generate such forces. The effect of these forces on the capture event depends on the phase relation of the two waves. Simple geometric considerations [15] concerning the kinematics of the bridge at low frequencies lead to the estimate that, when a wave in the bowing plane strikes the bridge, the reflected wave in the perpendicular plane can have an amplitude of up to one half of that of the reflected wave in the bowing plane. At higher frequencies more complicated behaviour occurs, which may be characterised by means of off-diagonal elements of the matrix of admittances at the bridge [17].

The details of the bow-force distribution will influence the local frictional behaviour, in particular the temporal and spatial distribution of slipping and sticking friction under the bow. Whether in general these perturbations of the bow force are advantageous in that they enrich the sound or detrimental in that they upset the establishment of Helmholtz motion is not clear.

The complex issue of the interaction of the two planes of vibration has received little attention to date. A further improvement of the model might be directed towards taking

into account the coupling of the motion in the bowing plane and the perpendicular plane through the action of the bow-hair. This is not an easy task, and may raise new questions regarding the microscopic details of the contact of bow-hair and string. Here, however, we regard bow-hair motion in the two planes as uncoupled.

6.1. Static bow-force distribution

For a given string we can calculate the distribution of the static bow force if we know the stiffness of the bow in this plane. In a simple experiment a bow was clamped at the frog and a force was applied to the bow-hair in the perpendicular plane. The measurements indicate that the total stiffness in the perpendicular direction can be modelled reasonably well by a linear spring. The measured spring constant $S_\perp$ varies from approximately 1000 N/m at 5 cm from the frog to approximately 100 N/m at 5 cm from the tip for a cheap and rather flexible bow, and probably twice those values for an acceptable bow. For the purpose of modelling, the spring constant is distributed according to $s_\perp = S_\perp / b$.

If longitudinal deformation of the string is neglected, the static deflection ζ of the string in the perpendicular plane is described by the ordinary differential equation,

$$T \frac{\mathrm{d}^2\zeta(x)}{\mathrm{d}x^2} - B \frac{\mathrm{d}^4\zeta(x)}{\mathrm{d}x^4} - f_\mathrm{b}(x) = 0, \qquad (3)$$

where T is the string tension and B its bending stiffness. The distributed bow force $f_\mathrm{b}(x)$ is zero everywhere except under the bow. Under the bow it is itself a function of the deflection of the string. Equation (3) must be solved for the two sections of free string and the section of the string under the bow. The solution, taking into account the possibility that the bow may be tilted, is described in the Appendix.

An example of such a calculation is given in Figure 17. The details of the model string are: diameter 1 mm, tension $T = 50$ N, length $l = 0.3$ m and Young's modulus $E = 1$ GPa, which corresponds to an inharmonicity parameter of $b_\mathrm{S} \approx 0.1$. The model bow has $b = 10$ mm, $S_\perp = 1000$ N/m and is positioned at $\beta = 1/10$. The total bow force is $F_\mathrm{b} = 3$ N, towards the upper limit of normal practice [18]. The computed string deflection for four different models is presented in Figure 17(a). The dotted lines correspond to the perfectly flexible string and the stiff string subject to a point load at the mid-point of the bow. The solid and the dashed lines show the two finite-width models: bending stiffness has a smaller effect than in the case of the point bow. Finally, the dash-dot line represents the case of the stiff string with the bow tilted at an angle of 30 degrees. The bow-force distributions are given in Figure 17(b). The distributions for the perfectly flexible and the stiff string are practically identical.

For tilted bows the calculation of the force distribution seems always worthwhile, although a linear force distribution is usually a good guess. For a bow placed flat on the string the non-uniformity in force is negligible unless $S_\perp$ is high (near the frog) or the string has a low tension force.

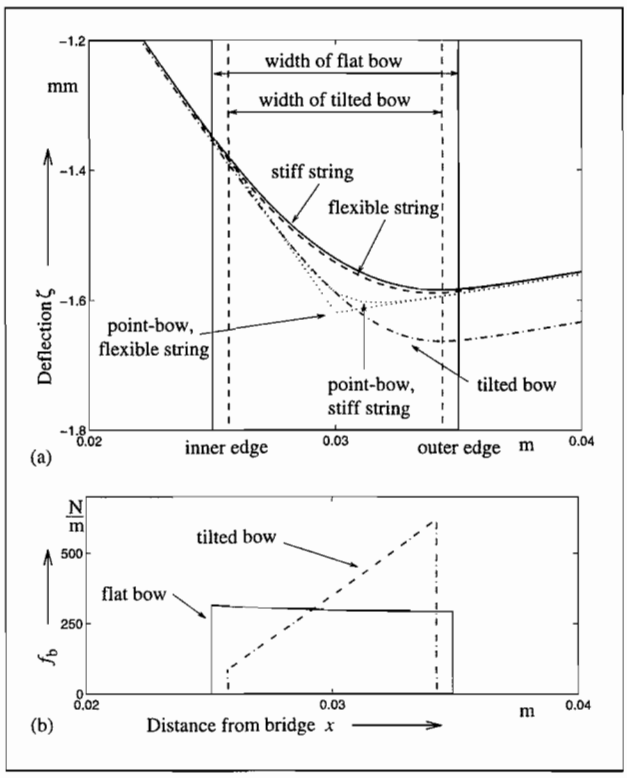

Figure 17. Computed string deflection (a) and bow-force distribution (b) in the perpendicular plane for various models. Solid line: stiff string under flat compliant finite-width bow. Dashed line: perfectly flexible string under same bow. Dash-dot line: stiff string, bow tilted at 30 degrees. Dotted lines: point-bow models.

Bending stiffness affects the string deflection under a compliant finite-width bow less than the corresponding point-bow calculations may lead one to expect.

6.2. Dynamic bow-force distribution

In this section we investigate theoretically the fluctuations of the bow force due to waves in the perpendicular plane incident on the bow. We adapt the analysis of the reflection and transmission problem of Part I Section 5 to the perpendicular plane. Imagine an infinite string in contact with a bow. Waves in the perpendicular plane travel to the bow, interact with it and generate a fluctuation F_b' of the bow force F_b. The theoretical results derived for the non-rolling motion in the bowing plane in Part I apply *verbatim* to the perpendicular plane. The impedance presented to the string by the bow is now the impedance in the perpendicular plane $Z_\perp$. In contrast to the case of the bowing plane, there is no nonlinear regime (slip) here. Therefore this study covers the physics of the perpendicular plane during the entire period of vibration.

The simplest case, that of a perfectly flexible string and a point bow has been investigated theoretically by Cremer [16]. For a perfectly flexible string with characteristic impedance Z_0 and a pure resistive bow impedance the greatest amount of energy dissipation occurs if $Z_\perp = -2Z_0$ (perfect impedance match and radiation condition). Half of the energy of the incident wave is dissipated.

ACUSTICA · acta acustica
Vol. 84 (1998)

For this situation, Cremer evaluates the effect of waves in the perpendicular plane on Helmholtz motion. He argues that $|F'_b/F_b|$ can be as large as 0.2 and that such fluctuations could have a considerable effect on the capture of the string. The effect on the release mechanism is likely to be smaller. The effect on capture is brought about by the transmitted wave which, after reflection at the nut, reaches the bow more or less simultaneously with the Helmholtz corner. The transmitted wave has a smaller amplitude than the original wave in the perpendicular plane and it is subject to rounding off while travelling between bow and nut.

We can now extend Cremer's investigation to a bow of finite width. A first attempt at assessing the effect of the modal behaviour of the ribbon of hair is also made. This seems relevant as measurements [19] of the frequency response of a cello bow driven on the bow-hair in the perpendicular plane show pronounced hair modes up to around 500 Hz.

To get an idea of the role of the modal structure of the frequency response, one may begin by modelling the bow-hair as a lossy stretched string. The frequency response of such a system is easily derived. Let the tension be T_H, the mass per unit length m_H and the length of the ribbon of hair l_H. We take damping into account in an *ad hoc* manner via a "complex tension" in the dispersion relation, the constant here being $T_H(1 + i\xi_\perp)$ with $\xi_\perp$ the loss factor. Point excitation is assumed at $\gamma\, l_H$ where γ denotes the relative distance of the excitation point from one end of the bow. The point input impedance is:

$$Z_\perp = \frac{i\, Z_{\perp\infty}}{2\sqrt{1+i\xi_\perp}} \frac{\sin k\, l_H}{\sin k\,\gamma\, l_H \,\sin k\,(1-\gamma)\, l_H}\,, \quad (4)$$

with

$$Z_{\perp\infty} = 2\sqrt{T_H\, m_H}\,, \quad (5)$$

$$k = \frac{\omega}{c}\,\frac{1}{\sqrt{1+i\xi_\perp}}\,, \quad (6)$$

$$c = \sqrt{\frac{T_H}{m_H}}\,. \quad (7)$$

For finite-width calculations an impedance per unit length is obtained through $z_\perp = Z_\perp/b$. Typical values for T_H, m_H and l_H are given in Table I. With these values and $\gamma = 0.5$ one finds lowest modes from around 70 Hz on violin bows to around 85 Hz on double-bass bows. This is in line with Askenfelt [20] and Schumacher [19] who, for violin and cello bows respectively, report the lowest bow-hair mode to be in the vicinity of 60–75 Hz.

We now need to quantify the loss factor. Energy is dissipated through internal friction within individual hairs and, as Ricca [21] reports, by the frictional interaction of neighbouring bow-hairs. How to model the combination of these mechanisms in any serious way is not clear. We can attempt to derive an estimate of the loss factor from Schumacher's ([19] Figure 1) measured frequency response function. This exhibits wide peaks and troughs but only a slow decrease in peak amplitude with mode number, and does not in fact fit our model, equation (4), very well. (A possible explanation lies in the influence of non-uniform tension forces among the individual hairs.) Matching theory and measurement in a very rough way gives $\xi_\perp \approx 0.1$, and we use this value in order to obtain preliminary results.

Table I. Data on bows. The quantities T_H, l_H, $M_H = m_H l_H$, $Z_{\perp\infty}$ and b are the hair tension force, the hair length between frog and tip, the mass of the ribbon of hair, the impedance of the bow hair and the average bow width.

Bow type	T_H [N]	l_H [m]	M_H [g]	$Z_{\perp\infty}$ [kg/s]	b [mm]
violin	60	0.65	4.5	1.3	10
viola	70	0.65	5.2	1.5	10
cello	90	0.61	6.2	1.9	12
bass	120	0.53	7.5	2.6	16

Two aspects of the results of the reflection and transmission calculations are worth discussing in detail. The first is the comparison of the force distributions in the two planes generated by incident waves: this allows us to assess the impact of waves in the perpendicular plane on Helmholtz motion. The second is the amplitude of the reflection coefficient in the perpendicular plane, since the waves reflected at the inner edge would have a directly audible effect when returning to the bridge.

The force fluctuations predicted by the point-bow and the finite-width models are compared in Figures 18(a)–(b) for incident unit amplitude waves with harmonic numbers 5 and 10. The model string is the one used throughout this paper. The forces f'_b calculated with the finite-width model are given by solid lines. The dashed lines show the forces F'_b resulting from the point-bow model, distributed across the width of the bow for presentational purposes. These are snapshots for phase angle $\pi/4$ when the forces are near their maxima. These snapshots convey the correct impression: the amplitudes of the finite-width forces are highest at the edge of the bow facing the incident wave.

For a large part of the relevant parameter range the point-bow force and the finite-width force, integrated over the bow width, have similar magnitudes and follow the same trends. However, since in the finite-width case the force is applied to a section of string rather than at a point, the same total force generates emitted waves with smaller amplitudes. This effect is strongest at high frequency. The finite-width model provides details of the force distribution and increased realism regarding the amplitudes of the waves emanating from the bow.

The predicted friction force, generated by the same wave now incident on the bow in the bowing plane, is shown in Figures 18(c)–(d). The amplitude of the friction force is also highest at the edge of the bow facing the incident wave. The strongly non-uniform distributions of both forces suggest that the point-bow argument underestimates the cross-effects between waves in the two planes.

In Figure 19 are shown the reflection coefficient and the total energy of the transmitted and reflected waves. These cal-

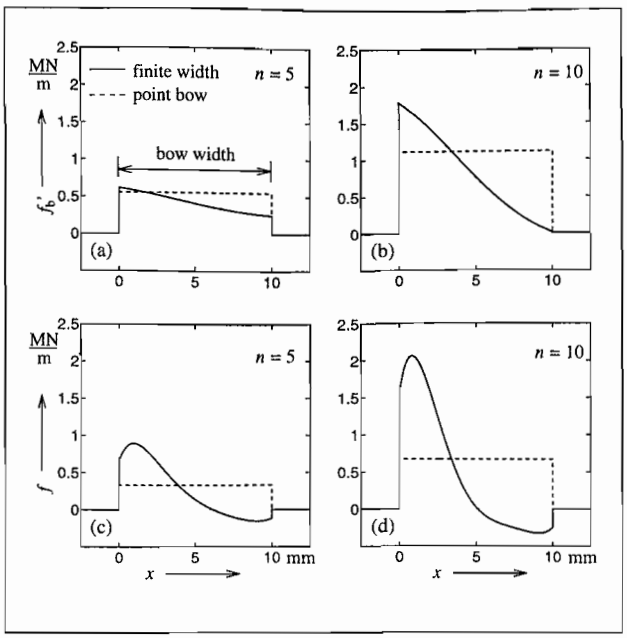

Figure 18. Force distributions (in MN/m) between bow and string for incident unit amplitude waves with harmonic numbers $n = 5$, 10 in the perpendicular and bowing plane. (a)–(b) bow-force fluctuation. (c)–(d) friction force for rolling string. Solid lines represent the finite-width model, dashed lines the point-bow model. For presentational purposes the point forces are distributed over the bow width. Violin bow according to Table I. Model string as used throughout.

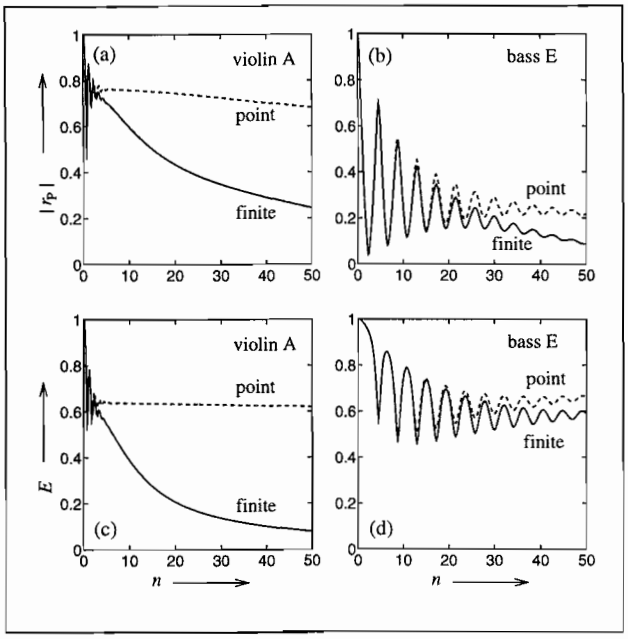

Figure 19. Reflection and transmission of waves in the perpendicular plane. Reflection coefficients versus harmonic number n for: (a) violin A string and (b) double-bass E string. Sum E of the kinetic energy of the reflected and transmitted waves normalised with the kinetic energy of the incident wave for: (c) violin A string and (d) double-bass E string. Solid lines finite-width model, dashed lines point-bow model.

culations are performed for the model string used throughout and for a model double-bass string as well, so as to cover the range of behaviour encountered among the instruments of the violin family. (The details of the double-bass string are given in Part I Table II.) The reflection and transmission behaviour in the perpendicular plane is a clear example of how the scaling of bows and strings differs within the violin family. The fundamental frequencies of the strings of the violin family range from 31–660 Hz, whereas the lowest bow-hair modes lies in the vicinity of 75 Hz for all bows of the violin family. In the case of the double-bass string bow-hair modes are visible throughout the relevant frequency range. In the case of the violin string, we find only vestiges of the modal properties of the bow, and this only at very low harmonic numbers.

The spreading of the bow-hair impedance in the finite-width model reduces the amplitude of the reflected wave. This is due to two effects: the finite-width bow is more permeable for incident waves and its dissipative effects are stronger. In the case of the point-bow model a maximum of 50% of the incident wave energy is dissipated (perfectly flexible string, pure resistive bow impedance). Greater dissipation is possible with a finite-width bow. Figures 19(c)–(d) give the energy of the outgoing waves normalised by the energy of the incident wave. With identical total impedance the finite-width bow dissipates significantly more energy. As the cases computed with the violin and the double-bass string indicate, low impedance strings are much more affected. Compared with the case of the rolling string treated in Part I losses are high because the mismatch of bow and string impedances is smaller and because the incident wave energy cannot be transmitted past the bow through the rolling mechanism. A simple qualitative experiment reported by Cremer [16] points in the same direction: a bow is placed on the string and the string is then plucked near the bow in both planes alternately. It appears that the tone generated by plucking in the perpendicular plane disappears first.

The effect of bending stiffness cannot be summarised in a simple way. Bending stiffness increases the transverse impedance of the string and can reduce the impedance mismatch of string and bow thus leading to higher dissipation. On the other hand bending stiffness can promote transmission past the bow (tunnelling). However, the overall conclusion echoes what was reported in Part I: the effect of bending stiffness is generally minor compared with that of bow-hair compliance.

6.3. Effect of tilting the bow

Players constantly adjust the angle at which the bow is tilted in the plane perpendicular to the bowing plane. A typical long down-bow stroke might start with the bow strongly tilted to ease the attack, after the initial transient the angle may be reduced and, as the tip of the bow is approached, the angle may be reduced even further. All this is done automatically as if there were immediate feedback from either the tone quality or the "feel" of the bow. The bows used on the instruments of the violin family are usually tilted in such a way that the value of the distributed bow force is reduced at the inner edge and increased at the outer edge. We refer to this direction

ACUSTICA · acta acustica
Vol. 84 (1998)

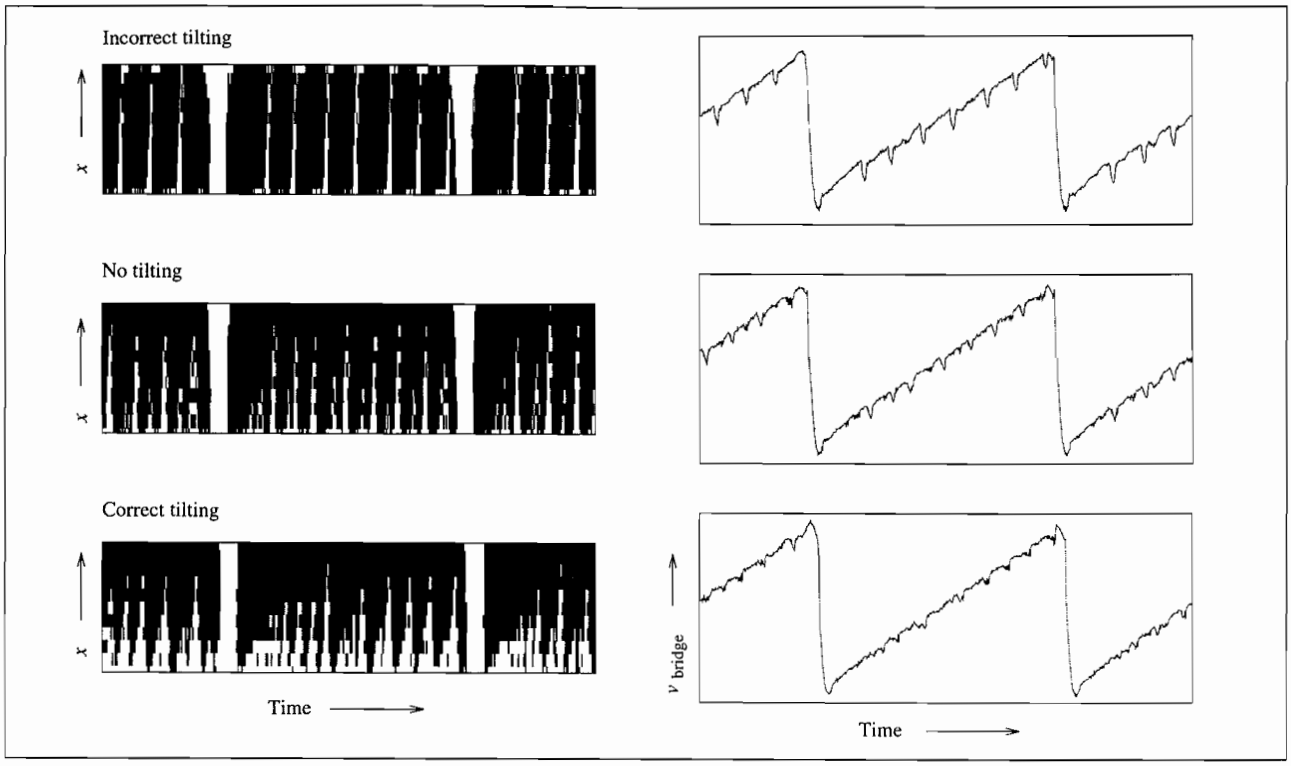

Figure 20. Friction maps and bridge-force waveforms for an incorrectly tilted, a flat and a correctly tilted bow. With $F_b = 1.5$ N throughout and $\epsilon = -1$, $\epsilon = 0$ and $\epsilon = 1$ respectively. Bow position $\beta = 1/23.2$.

of tilting as correct tilting. Note that because cellos (and double-basses) are played with the bridge end of the strings pointing away from the cellist, the cellist's bow hand rotates in the opposite direction to the violinist's bow hand in correct tilting, but the effect is the same in both cases.

There are two regimes of tilting: gentle tilting alters the distribution of the bow force whilst the full width of the ribbon of bow-hair remains in contact with the string; strong tilting means that only a fraction of the bow width is applied to the surface of the string. The distributed value of the bow force is then zero at one edge of the bow; in correct tilting this is the inner edge. Strong tilting thus defined is always associated with a small bow force, as a high bow force would again bring the full width of the bow in contact with the string or even allow the bow stick to touch the string.

We will assume simple bow-force distributions for the following examples of simulations results: uniform distribution for the case of the flat bow and a linear distribution for the tilted bow. All the important physical effects connected with tilting are covered by a linear distribution:

$$f_b(x) = \frac{F_b}{b}\left[1 + 2\epsilon\left(x - \frac{l\beta}{b}\right)\right] \qquad (8)$$

for $x \in [l\beta_i, l\beta_o]$ and $\epsilon \in [-1, 1]$.

Correct tilting corresponds to $\epsilon > 0$, a flat bow to $\epsilon = 0$ and incorrect tilting to $\epsilon < 0$. For the strongly tilted bow we have $\epsilon = 1$ and a reduced value of the bow width.

Figure 20 shows how tilting affects the contact mechanics in a case in which the string is bowed near the bridge with a rather high bow force. The β of the bow mid-point is $\beta = 1/23.2$ and the bow force is $F_b = 1.5$ N in all cases. The Schelleng maximum bow force is $F_{bS} = 1.7,\ 2.3,\ 3.5$ N for the values of β at the outer edge, the bow mid-point and the inner edge respectively. The middle diagram in Figure 20 shows the behaviour for the flat bow. Partial slips occur at both edges of the bow. The bridge-force waveform is moderately spiky. The top and bottom diagrams show the effects of incorrect and correct tilting respectively. Notice that when the bow is tilted in the incorrect sense, forward partial slips at the outer edge are more numerous and reach further into the bow. Also we find secondary slips extending over the full width of the bow and accordingly vigorous spikes in the bridge-force waveform. When the bow is tilted in the correct sense the forward partial slips no longer occur. The value of the bow force at the outer edge is now sufficiently high to maintain sticking throughout the nominal sticking phase of the Helmholtz cycle. The string element at the inner edge slips for the greater part of the cycle. A low bow force at the inner edge means a low threshold of limiting friction. Partial slips occurring at the inner edge under these circumstances have a reduced impact and generate smaller perturbations of the bridge-force waveform because the force impulse generated during the partial release is small. The duration of the stick-to-slip transition is dramatically shortened as the bow goes from incorrect to correct tilting (durations of 0.02, 0.01 and 0.005 T_0). The durations of ubiquitous slip and of the slip-to-stick transitions are much less affected in comparison.

In correct tilting the centre of gravity of the bow-force distribution is shifted towards the outer edge, where the Schel-

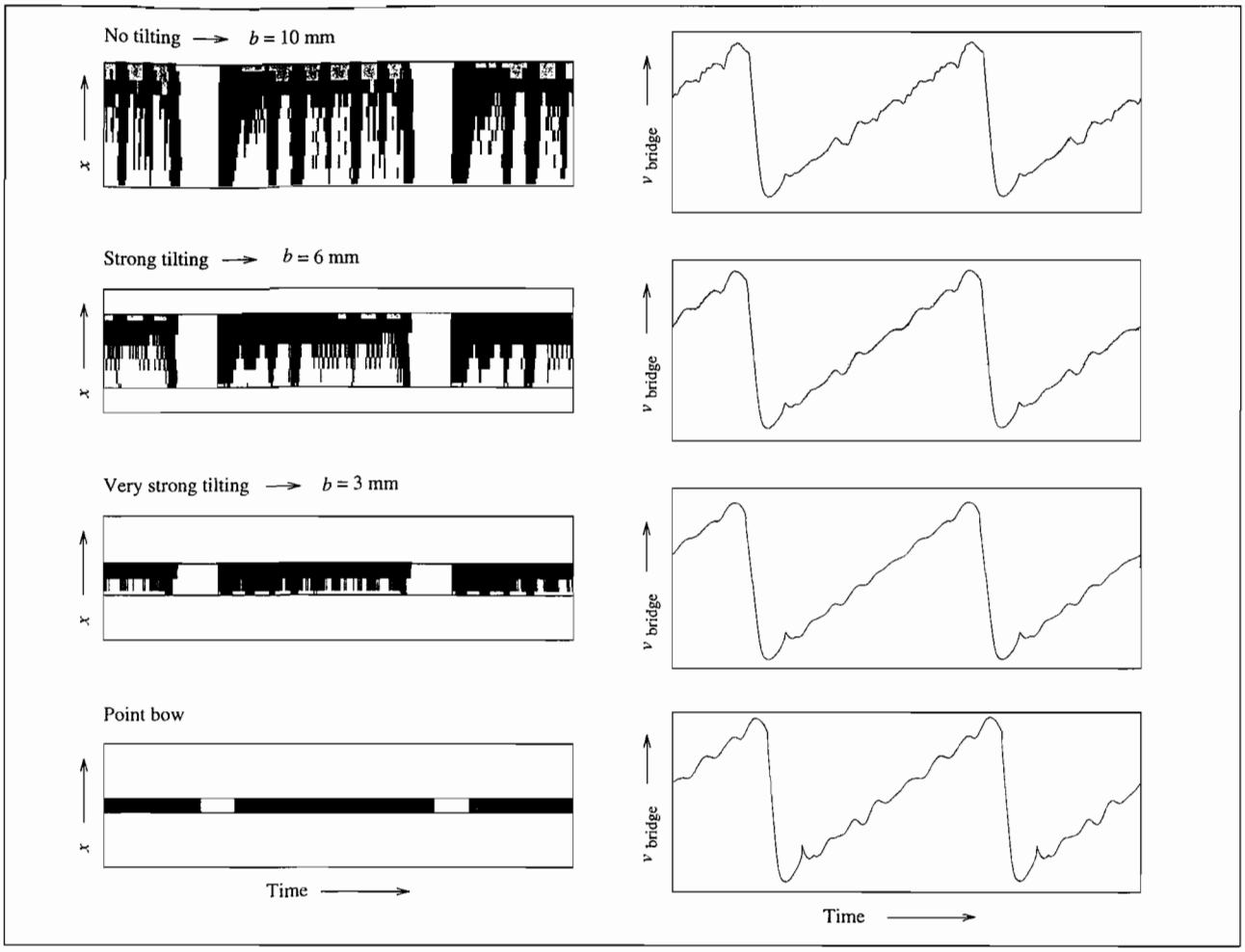

Figure 21. Strong tilting reduces the effective bow width. It is usually associated with small bow forces. Here $F_b = 0.2$ N and $\beta = 1/9.3$. The force distribution is linear with $\epsilon = 1$. The graphs of the fourth row are produced with the point-bow model.

leng maximum bow force F_{bS} is lower, $F_{bS} \approx F_b$ in the example discussed here. In incorrect tilting the centre of gravity of the bow-force distribution is shifted towards the inner edge, where the Schelleng maximum bow force is higher, $F_{bS} \approx 2F_b$. These shifts alone would lead us to believe that incorrect tilting is advantageous as it moves the effective bowing point into a position with a higher maximum bow force F_{bS}. Such finite-width effects highlight the limitations of Schelleng's maximum bow force rule. For fixed F_b and bow position β, the tilting angle alone can determine whether the waveforms generated represent acceptable or non-acceptable string motion.

For the investigation of strong tilting, bow widths of 10, 6 and 3 mm were chosen (see Figure 21). The mid-points of these model bows are located at $\beta = 1/9.3$, the β of the reference case. The same distributed value of the bow-hair impedance is used in all cases. In the point-bow case the distributed impedance of the 3 mm bow is lumped in one single point. A small bow force, $F_b = 0.2$ N, is used.

At the low bow forces associated with strong tilting the reduction in bow width is the important consequence of tilting rather than the redistribution of the bow force. With decreasing bow width the degree of incompatibility between string and bow velocity is reduced, which means fewer and less vigorous partial slips. Accordingly the bridge-force waveform is rendered smoother. The details of the bow force distribution play an increasingly small role as the bow width is decreased. Incorrect tilting would change the friction maps of the 6 mm and the 3 mm cases but would leave the bridge-force waveforms virtually unaffected. This is not to say that finite width does not matter when b is small: note the differences in bridge-force waveforms of the 3 mm case and the point-bow case.

Viol players usually tilt the bow in the direction referred to here as incorrect tilting. This tilting direction is in fact dictated by the way the viol bow is conventionally held in the hand. It can be argued that viols are played using bow forces smaller than those used on instruments of the violin family. Viol bows are softer: the bow stick is weaker, the ribbon of bow-hair consists of fewer hairs and is narrower, and the ribbon of hair is not restricted laterally at the frog by a ferrule as it is on the bows of the violin family. All these facts support the view that tilting, apart from reducing the effective bow width, is likely to have very little effect in viol playing. The tilting direction may therefore be largely immaterial.

ACUSTICA · acta acustica
Vol. 84 (1998)

7. Conclusions

In this paper and its two predecessors [1, 2], models have been developed for the detailed behaviour of a string in contact with a bow over a finite region. These models have been applied to problems of reflection and transmission of incident waves on the string, and to self-sustained motion of a bowed string. Results have been compared and contrasted with those obtained using the more familiar point-contact models. The overall conclusion is that point-bow and finite-width models produce distinctly but not fundamentally different behaviour. This conclusion is not self-evident and is a result in itself. However, the knowledge of the physics of the bowed string acquired from point-bow models needs amending in a number of ways. Many physical effects can be generated with both models but these effects appear in different parts of the parameter space. Other effects are only accessible with finite-width modelling.

Finite-width simulations give valuable insight into the contact mechanics of bow and string. In most linear problems point and finite-width excitation deliver qualitatively similar answers when the region of excitation is small compared with the size of the vibrating system, and with the wavelength of disturbances generated. This is not the case for a bowed string. The choice between sticking and sliding friction, and the value of the friction force, is governed by local conditions at each point in the contact region. The friction force at any particular point need not follow the time-dependence of the force in a corresponding point-bow model. Neither need the *average* friction force in the finite-width model follow this point-bow behaviour. Thus, bowed-string models with point and finite-width excitation, using the same friction law, can give rather strongly differing answers. Clear examples are given by the phenomenon of partial slipping, and by the strong differences in flattening and maximum bow force predicted by corresponding point-bow and finite-width models as discussed in Section 2.

To obtain correct predictions of the detailed behaviour in such cases, there is no doubt that finite-width modelling is necessary. However, such modelling is computationally much more demanding than point-bow modelling, so it makes sense to ask whether there is in any sense an "equivalent point-bow model" to a given finite-width model, which gives a better match of behaviour. A simple approach is to fit a point-bow friction law to the variation of the averaged friction force in the finite-width model. The most important difference is that the limiting coefficient of sticking friction is significantly reduced by the averaging process, since different points in the contact region experience the maximum force at different times. We have shown that such a modified friction law leads to much better agreement between the two types of models with regard to both the flattening effect and the maximum bow force. In fact, the flattening effect may be an interesting subject for an experimental investigation of the role of finite bow width.

The particular issue of detecting the maximum bow force in finite-width simulations draws attention to the non-trivial question of how to distinguish, in computed waveforms, musically-acceptable string motion from unacceptable motion. Partial slips are a ubiquitous phenomenon in finite-width simulations: sometimes quasi-periodic, sometimes quite irregular. These partial slips produce spikes in the bridge-force waveform, and hence would have directly audible consequences in the radiated sound from the instrument. The limit of musical acceptability will depend in some way on the magnitude, timing, and detailed shape of these spikes, and no doubt also on the musical context. The conditions under which the pattern of spikes becomes significantly aperiodic has been examined. It appears likely that this condition might be strongly affected by temporal variation of the bow force due to, for example, bow and string vibration in the plane perpendicular to the bowing plane. To draw the line of musical acceptability might require us to take account of these temporal variations.

To make physical sense, a finite-width model of the bow and string contact must take bow-hair compliance into account because the assumption of a rigid bow implies non-physical, singular friction forces at the edges of the bow. The oscillation regimes produced by finite-width simulations show sensitivity to the value of the bow-hair compliance, and this sensitivity is stronger than that shown by point-bow simulations. Point-bow simulations do not require bow compliance to produce sensible results, and perhaps this fact has encouraged the erroneous conclusion that bow compliance is of little importance in bowed-string motion. The range of possible values of the bow compliance has been narrowed down by measurements on single bow-hairs, by testing a mathematical model for bow-hair behaviour against experimental data in the context of the Eisenberg-Cremer reflection and transmission experiment, and finally by investigating the range of bow compliance which is "playable" in finite-width simulations of the bowed string. The level of bow-hair damping has also been found to play a decisive role in the behaviour of the finite-width model. A worthwhile goal of further research would be to design and carry out experiments to determine the elastic and damping behaviour of bow-hair to greater accuracy.

The study of the reflection and transmission problem in Part I suggested that bending stiffness of the string plays a secondary role in the contact mechanics, and is only noticeable when the string is so stiff that its inharmonicity may become unacceptable. Bowed-string simulations produce a rather similar conclusion, but the effect of bending stiffness can be magnified in the details of the stick-to-slip and slip-to-stick transitions. The effect of bending stiffness in the vicinity of the bow acts in opposition to the flattening effect.

There seems to be a good reason for tilting the bow so that it does not lie flat on the string, and also for the conventional direction of this tilt. Tilting of the bow reduces the amplitude and sharpness of secondary waves generated by partial slips and can thereby allow Helmholtz motion to continue to exist at higher bow force levels. At low bow force the main effect of tilting seems to be a reduction in bow width with the consequences described in Section 2.

The detailed theoretical study of dynamic effects in the perpendicular plane suggests that fluctuations of the bow

force can have a stronger impact on established Helmholtz motion than a point-bow approach would lead us to expect. A reflection and transmission experiment involving only waves in the perpendicular plane might yield some insight into these effects, which in turn might help understand time-variations in waveforms observed in the bowing plane. Such experiments would also be likely to provide some information on bow-hair damping due to hair interaction.

This study has examined only simulations which were initialised with ideal Helmholtz motion, to explore the effect of contact dynamics on more-or-less periodic motions of the string. The much more complicated area of transient behaviour of finite-width models has not received any attention so far. Systematic studies of simulations of initial transients using point-bow models [22, 9, 23] have shown that the "pattern-selection process" which determines whether for a given bow velocity and bow force transient the string settles down to Helmholtz motion or not, and if so, how quickly, is very sensitive to changes in the playing parameters, the frictional behaviour, and the parameters describing the mounted string and the bow. It seems safe to anticipate that finite-width effects will also play a strong role in transient behaviour. This is a topic for future research.

Appendix

Static bow-force distribution

Imagine a bow tilted at an angle α, defined as the angle between the undeflected ribbon of bow-hair and the undeflected string (see Figure 16). For the tilted bow one might not apply the full width of the ribbon of hair to the surface of the string. Let b and b^* be the full and the actually applied bow width respectively. If the bow force is sufficiently high to bring all hairs of the tilted bow in contact with the string, $b^* \approx b$; otherwise $b^* < b$, and b^* becomes an unknown of the system.

For $\alpha = 0$ the spring stiffness of the bow in z-direction $S_\perp$ is easily measured (Section 6). As above the corresponding distributed quantity is assumed to be $s_\perp = S_\perp / b$. Since the bow stick is axisymetric in cross-section it is reasonable to assume that the distributed spring stiffness for $\alpha \neq 0$ is also $s_\perp$.

Let the length of the string be l. Let the inner edge, the midpoint and the outer edge of the bow have the x-coordinates $x = \beta_\mathrm{i}\, l$, $x = \beta\, l$ and $x = \beta_\mathrm{o}\, l$ with respect to the bridge. One can derive a simple expression linking the distributed bow force and the deflection of the string:

$$f_\mathrm{b}(x) = s_\perp \left[\zeta_0 + (\beta_\mathrm{o}\, l - x)\, \tan\alpha - \zeta(x)\right] \quad \text{(A1)}$$

for $x \in [\beta_\mathrm{i}\, l, \beta_\mathrm{o}\, l]$, and $f_\mathrm{b}(x) = 0$ elsewhere. If the string (and thereby the load on the hair) were removed, the ribbon of bow-hair would form the straight line defined by $\zeta(x) = \zeta_0 + (\beta_\mathrm{o}\, l - x)\, \tan\alpha$. The position of the outer bow-hair would be ζ_0.

The task is now to find ζ_0 and $\zeta(x)$ and, if $b^* \neq b$, also b^*, for a given choice of the player's parameters total bow force F_b, tilting angle α and relative bow position β_o. Equation (3) is integrated for the two sections of free string on either side of the bow and the section of string under the bow. The general solutions are

$$\zeta_\mathrm{I}(x) = C_1 e^{\gamma_1 x} + C_3 e^{\gamma_2 x} + C_3 x + C_4, \quad \text{(A2)}$$

$$\zeta_\mathrm{III}(x) = C_9 e^{\gamma_1 x} + C_{10} e^{\gamma_2 x} + C_{11} x + C_{12}, \quad \text{(A3)}$$

$$\text{with} \qquad \gamma_{1,2} = \pm\sqrt{\frac{T}{B}} \quad \text{(A4)}$$

for the sections of free string, and

$$\zeta_\mathrm{II}(x) = \zeta_0 + (\beta_\mathrm{o}\, l - x)\, \tan\alpha + C_5 e^{\gamma_5 x} + C_6 e^{\gamma_5 x} + C_7 e^{\gamma_7 x} + C_8 e^{\gamma_8 x} \quad \text{(A5)}$$

$$\text{with } \gamma_{5-8} = \pm\sqrt{\frac{1}{2}\frac{T}{B}\left(1 \pm \sqrt{1 - \frac{4 s_\perp B}{T^2}}\right)} \quad \text{(A6)}$$

for the section of the string under the bow, where C_1–C_{12} are the integration constants. Together with the boundary and the continuity conditions this leads to 12 equations for the 12 integration constants.

Since the bow force is an integral quantity it cannot be inserted into the calculation directly as a given parameter and iteration is required. For the flat bow one can choose a value of ζ_0, compute the string deflection and the force distribution and integrate the distributed force over the width of the bow to obtain the total bow force, the quantity one is accustomed to in the discussion of the bowed string. For a given total bow force F_b, a plausible estimate of ζ_0 is

$$\zeta_0 \approx \frac{F_\mathrm{b}}{T}\, \beta_\mathrm{o}(1 - \beta_\mathrm{o})\, l + \frac{F_\mathrm{b}}{s_\perp b}, \quad \text{(A7)}$$

the sum of the deflection due to an equivalent point force on the perfectly flexible string at $x = \beta_\mathrm{o} l$ and the deflection of the bow-hair thought of as a lumped spring. Through variation of ζ_0 one finds the regime in which the resulting bow force matches the given bow force.

For the tilted bow the procedure is more involved: the *a priori* unknown value of the actual bow width corresponding to a given total bow force determines the x-coordinate of the interface between the section of string under the bow and the section of free string on the bridge side. One has to perform an iterative calculation starting from physically sensible first estimates of b^* and $\zeta(x)$ under the bow.

The assumption that the section of the string under the bow is horizontal leads to a useful first approximation for the actual bow width b^*:

$$b^* \approx \sqrt{\frac{2 F_\mathrm{b}}{s_\perp \tan\alpha}} \quad \text{if } F_\mathrm{b} \leq \frac{1}{2} s_\perp b^2 \tan\alpha,$$

$$b^* \approx b \quad \text{if } F_\mathrm{b} \geq \frac{1}{2} s_\perp b^2 \tan\alpha.$$

The estimate of the bow width together with the tilting angle provides an estimate of the bow-hair deflection. For an estimate of ζ_0 the value of the bow-hair deflection at the outer

ACUSTICA · acta acustica
Vol. 84 (1998)

hair is added to the deflection of the perfectly flexible string under a point load acting at $x = \beta_0 l$. Once the iteration is completed and the string deflection is known, the bow force distribution is simply calculated from equation (A1).

References

[1] R. Pitteroff, J. Woodhouse: Mechanics of the contact area between bow and string. Part I: Reflection and transmission behaviour. Acustica - acta acustica (1998). in preparation.
[2] R. Pitteroff, J. Woodhouse: Mechanics of the contact area between bow and string. Part II: Simulating the bowed string. Acustica - acta acustica (1998). in preparation.
[3] H. Bouasse: Mouvement des cordes sous l'archet. – In: Cordes et membranes. Delgrave, Paris, 1926.
[4] C.-A. Faure, X. Boutillon: Détermination et étude expérimentale de la fréquence d'oscillation d'une corde frottée. C. R. Acad. Sci. Paris **317** (1993) 1377–1382.
[5] R. T. Schumacher: Measurements of some parameters of bowing. J. Acoust. Soc. Am. **96** (1994) 1985–1998.
[6] M. E. McIntyre, J. Woodhouse: On the fundamentals of bowed-string dynamics. Acustica **43** (1979) 93–108.
[7] X. Boutillon: Analytical investigation of the flattening effect: The reactive power balancing rule. J. Acoust. Soc. Am. **90** (1991) 754–763.
[8] K. Guettler: The bowed string computer simulated — some characteristic features of the attack. Catgut Acoust. Soc. Journal **2** (1992) 22–26.
[9] R. T. Schumacher, J. Woodhouse: The transient behaviour of models of bowed-string motion. Chaos **5** (1995) 509–523.
[10] W. Güth: Zur Bogenanregung bei Streichinstrumenten. Acustica **80** (1994) 166–169.
[11] M. Kimura: "Subharmonics": An extended technique for the violin. J. Acoust. Soc. Am. **97** (1995) 3270.
[12] R. J. Hanson, A. J. Schneider, F. W. Halgedahl: Anomalous low-pitched tones from a bowed violin string. Catgut Acoust. Soc. Journal **2** (1994) 1–7.
[13] K. Guettler: Wave analysis of a string bowed to anomalous low frequencies. Catgut Acoust. Soc. Journal **2** (1994) 8–14.
[14] J. C. Schelleng: The bowed string and the player. J. Acoust. Soc. Am. **53** (1973) 26–41.
[15] C. Gough: The nonlinear free vibration of a damped elastic string. J. Acoust. Soc. Am. **75** (1984) 1770–1776.
[16] L. Cremer: The physics of the violin. MIT Press, Cambridge, MA, USA, 1985.
[17] X. Boutillon, G. Weinreich: Measurement of the three-dimensional admittance at a violin bridge. Proceedings 13th ICA Belgrad, Yugoslavia, 1989. 87–90.
[18] A. Askenfelt: Measurement of bowing motion and bow force in violin playing. J. Acoust. Soc. Am. **80** (1986) 1007–1015.
[19] R. T. Schumacher: Some aspects of the bow. Catgut Acoust. Soc. Newsletter **24** (1975) 5–8.
[20] A. Askenfelt: Observations on the dynamic properties of bows. Speech Transmission Quarterly Progress and Status Report, Royal Institute of Technology, Stockholm **4** (1992) 43–49.
[21] B. Ricca: Measurements of the impedance presented by a bow to a bowed string. Dissertation. University of Michigan, 1992.
[22] J. Woodhouse: On the playability of violins. Part II: Minimum bow force and transients. Acustica **78** (1993) 137–153.
[23] R. T. Schumacher, J. Woodhouse: Computer modelling of violin playing. Contempory Physics **36** (1995) 79–92.